

New Rhodamine Nitroxide Based Fluorescent Probes for Intracellular Hydroxyl Radical Identification in Living Cells

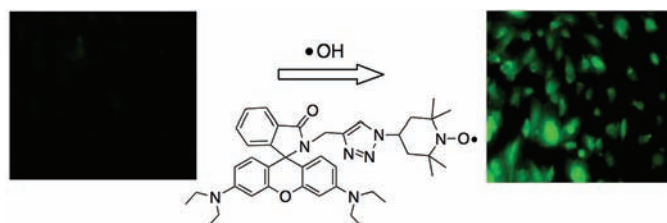
Nazmiye B. Yapici,[†] Steffen Jockusch,[§] Alberto Moscatelli,[§] Srinivas Rao Mandalapu,[†] Yasuhiro Itagaki,[§] Dallas K. Bates,[†] Sherri Wiseman,[‡] K. Michael Gibson,^{*,‡} Nicholas J. Turro,^{*,§} and Lanrong Bi^{*,†}

Department of Chemistry and Department of Biological Sciences, Michigan Technological University, Houghton, Michigan 49931, United States, and Department of Chemistry, Columbia University, 3000 Broadway, New York, New York 10027, United States

*lanrong@mtu.edu (L.B.); kmgibson@mtu.edu (K.M.G.); njt3@columbia.edu (N.J.T.)

Received October 19, 2011

ABSTRACT



The synthesis, characteristics, and biological applications of a series of new rhodamine nitroxide fluorescent probes that enable imaging of hydroxyl radicals ($\bullet\text{OH}$) in living cells are described. These probes are highly selective for $\bullet\text{OH}$ in aqueous solution, avoiding interference from other reactive oxygen species (ROS), and they facilitate $\bullet\text{OH}$ imaging in biologically active samples. The robust nature of these probes (high specificity and selectivity, and facile synthesis) offer distinct advantages over previous methods for $\bullet\text{OH}$ detection.

Reactive oxygen species (ROS) are associated with numerous pathologies including neurodegenerative diseases, ischemic or traumatic brain injury, cancer, diabetes, liver injury, and AIDS.¹ The primary ROS include the hydroxyl radical, superoxide anion, and hypochlorite radical. Of the preceding, the hydroxyl radical ($\bullet\text{OH}$) holds an important role in relation to its high reactivity. Essentially all biomacromolecules are susceptible to damage from $\bullet\text{OH}$, including carbohydrates, nucleic acids, lipids, and amino acids² making it one of the most deleterious intracellular ROS. The ability to detect and quantify intra- and extracellularly generated $\bullet\text{OH}$ yields

key information about the location and extent of redox damage and provides clues to the resulting cellular response. Accordingly, methods that are sensitive, accurate, and reproducible for the detection of $\bullet\text{OH}$ provide an important tool for understanding pathophysiology in a host of inherited and acquired diseases. A frequently

[†] Department of Chemistry, Michigan Technological University

[§] Department of Chemistry, Columbia University.

[‡] Department of Biological Sciences, Michigan Technological University.

(1) Dalle-Donne, I.; Rossi, R.; Colombo, R.; Giustarini, D.; Milzani, A. *Clin. Chem.* **2006**, *52*, 601.

(2) Halliwell, B.; Gutteridge, J. M. C. *Free Radicals in Biology and Medicine*, 2nd ed.; Oxford University Press: New York, 1989.

(3) (a) Yang, X. F.; Guo, X. Q. *Analyst* **2001**, *126*, 1800. (b) Li, B. B.; Gutierrez, P. L.; Blough, N. V. *Anal. Chem.* **1997**, *69*, 4295. (c) Tang, B.; Zhang, L.; Geng, Y. *Talanta* **2005**, *65*, 769. (d) Ischiropoulos, H.; Gow, A.; Thom, S. R.; Kooy, N. W.; Royall, J. A.; Crow, J. P. *Methods Enzymol.* **1999**, *301*, 367. (e) Lebel, C. P.; Ischiropoulos, H.; Bondy, S. C. *Chem. Res. Toxicol.* **1992**, *5*, 227. (f) Ohashi, T.; Mizutani, A.; Murakami, A.; Kojo, S.; Ishii, T.; Taketani, S. *FEBS Lett.* **2002**, *511*, 21. (g) Wardman, P.; Burkitt, M. J.; Patel, K. B.; Lawrence, A.; Jones, C. M.; Everett, S. A.; Vojnovic, B. *J. Fluoresc.* **2002**, *12*, 65. (h) Myhre, O.; Andersen, J. M.; Aarnes, H.; Fonnum, F. *Biochem. Pharmacol.* **2003**, *65*, 1575. (i) Tang, B.; Li, P.; Xie, T.; Duan, X.; Yu, F. B.; Wang, X. *Chem.—Eur. J.* **2010**, *16*, 1834. (j) Setsukinai, K.; Urano, Y.; Kakinuma, K.; Majima, H. J.; Nagano, T. *J. Biol. Chem.* **2003**, *278*, 3170. (k) Soh, N.; Makiyama, K.; Ariyoshi, T.; Seto, D.; Maki, T.; Nakajima, H.; Nakano, K.; Imato, T. *Anal. Sci.* **2008**, *24*, 293. (l) Lin, W. Y.; Yuan, L.; Song, J. Z. *Chem. Commun.* **2010**, *46*, 7930.

used approach for detecting $\bullet\text{OH}$, electron spin resonance (ESR) spectroscopy is limited by low spatial resolution and, thus, cannot be applied to real-time imaging of $\bullet\text{OH}$ in individual cells. To overcome this limitation, other investigators have employed fluorescent probes coupled to ESR in order to enhance both sensitivity and spatial resolution needed for intracellular detection of $\bullet\text{OH}$.³

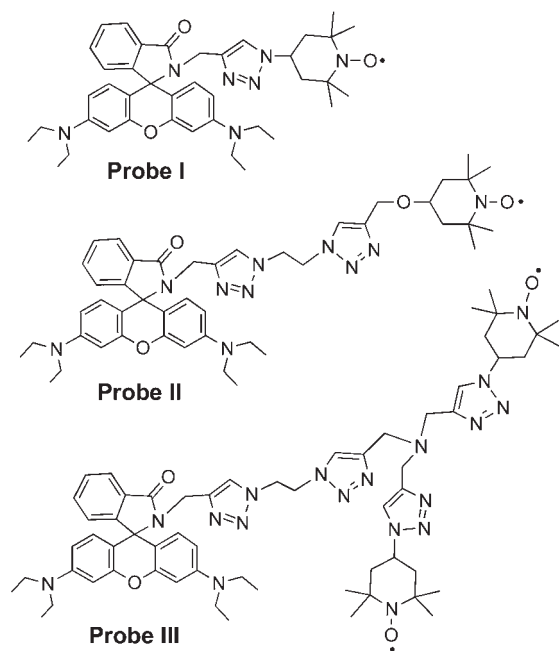


Figure 1. Rhodamine nitroxide based fluorescent probes I–III.

Nonetheless, the practical applications for fluorescent-ESR probes in biological systems are limited by the co-occurrence of cell damage, autofluorescence, and interference from other ROS. We sought to overcome these limitations through the development of a nonredox mechanism for $\bullet\text{OH}$ detection that eliminates ROS interferences and facilitates high specificity. Our novel approach for $\bullet\text{OH}$ imaging employs fluorogenic spin probes that can be detected by both fluorescence and EPR spectroscopy. The rhodamine nitroxide probe represents a non-fluorescent species that quantitatively reacts with $\bullet\text{OH}$ in DMSO solution to produce highly fluorescent products with absorbance/emission maxima at 560/588 nm. Because the reaction mechanism is not redox-based, we hypothesized that these probes would be selective. Moreover, the long wavelength emission spectrum of the fluorescent product minimizes interference from autofluorescence that exists in the majority of biological samples and mostly appears at shorter wavelengths. The current report describes the synthesis, spectroscopic characteristics, and imaging features of a new series of highly selective $\bullet\text{OH}$ -responsive fluorescent probes (I–III) (Figure 1) that we predict will significantly advance the field of intracellular $\bullet\text{OH}$ imaging.

Design and Synthesis of the Rhodamine Nitroxide Based Dual Probes for Hydroxyl Radical Detection. Synthesis of

molecular probes I–III was accomplished using sequential “click” reactions under mild conditions (Scheme S1, Supporting Information). In order to prevent fluorophore/nitroxide cleavage, the nitroxide is introduced into the molecular probe via the “click” reaction. To avoid reduction of the nitroxide to the nonparamagnetic hydroxylamine derivative by sodium L-ascorbate during the click reaction, copper(I) iodide (10 mol %) has been employed as the copper(I) source instead of the more common Cu(II)SO_4 /sodium L-ascorbate system. All intermediates were characterized by ^1H and ^{13}C NMR, and the structural characteristics of all target compounds were confirmed by high-resolution mass spectrometry. Because of the observed paramagnetic broadening caused by the free radical, probes I–III were additionally treated with sodium L-ascorbate to generate the corresponding hydroxylamines (nonradical), which facilitated characterization by ^1H and ^{13}C NMR. The nitroxide-labeled probes were also analyzed by EPR spectroscopy to confirm the intact nitroxide label. Probes I–III are stable and were stored at room temperature in sealed and light-protected bottles until use.

Spectroscopic Properties and Response to $\bullet\text{OH}$. We employed the Fenton reaction to generate $\bullet\text{OH}$, at pH 4.0, a pH supporting optimal Fenton oxidation.⁴ Spectral characteristics of probes I–III were tested following reaction with $\bullet\text{OH}$ generated from the Fenton reaction. Figures 2 and S1 describe typical absorbance/fluorescence spectra for probes I–III in the absence and presence of a Fenton reagent. Probes I–III in their lactam form show only weak absorbance and almost no fluorescence. After addition of the Fenton reagent $\bullet\text{OH}$ are generated, which can react with DMSO, which is present in the solution, to generate methyl radicals ($\bullet\text{CH}_3$). Subsequently, $\bullet\text{CH}_3$ can react efficiently with the nitroxide radical of the probes, which leads to a diamagnetic compound, thereby eliminating intramolecular quenching and resulting in enhanced fluorescence. In addition, the low pH (pH = 4) opens the lactam leading to strongly absorbing rhodamine chromophores.

Next, we subsequently monitored the changes in fluorescence spectra of our probes in the presence of differing $\bullet\text{OH}$ concentrations. The concentration of $\bullet\text{OH}$ is directly proportional to the Cu^{2+} concentration. Figure S2 depicts the fluorescence responses of probes I–III to the presence of $\bullet\text{OH}$. When simultaneously added to probes I–III, the Fenton reagent and DMSO yielded an immediate increase in fluorescence intensity. For example, incubation of probe III with Fenton reagent/DMSO led to an ~ 400 -fold increase in fluorescence intensity, and this fluorescence intensity increased in parallel with the increase of the Fenton reagent concentration. When the $\bullet\text{OH}$ concentration exceeds $33 \mu\text{M}$, however, the fluorescence intensity displayed saturation indicating that essentially all of probe III ($1 \mu\text{M}$) had reacted with $\bullet\text{OH}$.

(4) (a) Kwon, B. G.; Lee, D. S.; Kang, N.; Yoon, J. *Water Res.* **1999**, *33*, 2110. (b) Nogueira, R. F. P.; Guimaraes, J. R. *Water Res.* **2000**, *34*, 895. (c) Kang, Y. W.; Hwang, K. Y. *Water Res.* **2000**, *34*, 2786.

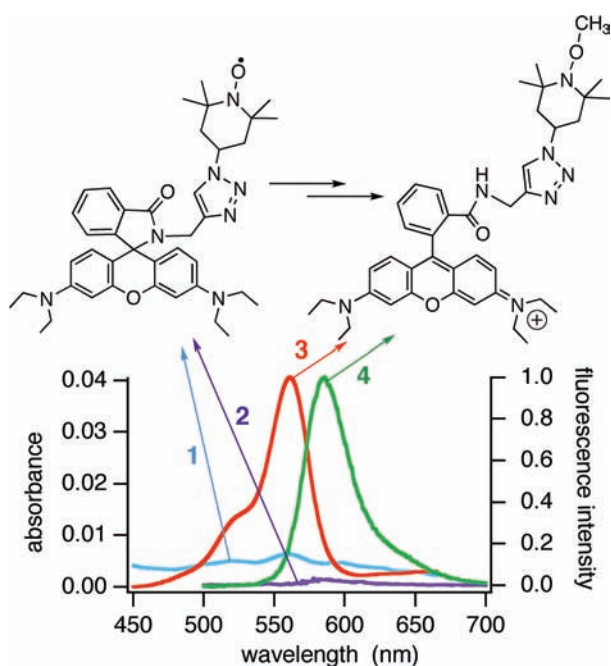


Figure 2. Absorbance (line 1, 3) and fluorescence spectra (line 2, 4) of probe I ($1 \mu\text{M}$) before (line 1, 2) and after (line 3, 4) addition of Fenton reagent ($\text{Cu}^{2+}:\text{H}_2\text{O}_2$, mol/mol = 1:30) in the presence of DMSO (0.1%) at pH = 4.

The highest fluorescence enhancement seen with probe III was most likely associated with its binitroxide structure. Unique to our strategy, a dark background from which a bright signal appears upon reaction with $\bullet\text{OH}$ offers a distinct advantage in comparison to other probes for $\bullet\text{OH}$,³ and the correspondingly decreased background fluorescence lends itself to a higher signal-to-noise ratio, a highly desirable end point for *in vivo* imaging with live cells.

We exposed our probes to a variety of radical species. Our results revealed that probe III exhibited a >1000-fold higher response for $\bullet\text{OH}$ in comparison to NO, H_2O_2 , and glutathione and a >40-fold higher response for $\bullet\text{OH}$ over $\text{ROO}\bullet$, ascorbate, SIN-1, and superoxide. Probes I and II also demonstrated selectivity for $\bullet\text{OH}$ versus other ROS (Figure S3–S4). We suggest that the selectivity of these probes for $\bullet\text{OH}$ results from the high reactivity of $\bullet\text{OH}$ with any organic molecules (such as DMSO present in our experiments) to generate carbon centered radicals by H-abstraction, which subsequently react with the nitroxides. The other ROS have lower rate constants of direct reaction with nitroxides and lower rate constants of H-abstraction from organic molecules to generate carbon centered radicals.

In Vivo Detection of $\bullet\text{OH}$ during Oxidative Stress. Since retinal pigment epithelial cells are susceptible to oxidative damage,⁵ we employed ARPE-19 cells (human retinal

pigment epithelial cells) to examine the capacity of our probes to measure $\bullet\text{OH}$ generated in an active biological environment. Incubation of ARPE-19 cells with probe I, II, or III ($2 \mu\text{M}$) for 12 h at 37°C yielded negligible intracellular background fluorescence (Figure S5). Conversely, addition of $10 \mu\text{M}$ $\bullet\text{OH}$ to probe-loaded cells (12 h, 37°C) triggers a considerable increase in intracellular fluorescence. Also, determination of DIC (differential interference contrast) images and nuclear counter staining confirmed that our cells were viable throughout the imaging analyses, all of which indicated that our probes were cell permeable, nontoxic, and capable of detecting increased $\bullet\text{OH}$ under conditions indicative of oxidative stress.

Iron or copper can induce production of $\bullet\text{OH}$ from H_2O_2 . Accordingly, we extended the previous studies and further induced oxidative stress using hydrogen peroxide. Exposure of probe (I–III)-preloaded ARPE-19 cells resulted in considerable fluorescence induction following H_2O_2 exposure (Figure S6), and the time-related increase in fluorescence suggested ongoing reaction of the probe with additional radicals. As a control for this experiment, cells were exposed to oxidative stress conditions in the absence of the probes, and the weak autofluorescence indicated that enhanced fluorescence with peroxide addition correlated with increased $\bullet\text{OH}$ concentration.

Low-Level Detection of $\bullet\text{OH}$ with PMA (12-Myristate 13-Acetate) Stimulation. To test the sensitivity of our probes detecting the concentrations of $\bullet\text{OH}$ produced with physiological stimulation (very low levels expected in signaling cascades), we employed ARPE-19 cells which are predicted to generate low micromolar levels of $\bullet\text{OH}$ upon stimulation with PMA.⁶ Accordingly, ARPE-19 cells were stimulated with PMA (40 ng/mL) and incubated with probes I–III ($2 \mu\text{M}$) for 12 h (Figure 3). ARPE-19 cells incubated with $2 \mu\text{M}$ probes I–III revealed minimal background fluorescence. Conversely, a striking increase in intracellular fluorescence was observed upon treatment of probe I–III- ($2 \mu\text{M}$) preloaded cells with PMA. Control experiments with cells in the absence of either probe or a probe without PMA stimulation yielded negligible fluorescence responses. Moreover, cellular viability was verified with DIC images. These findings indicate that probes I–III are both cell membrane-permeable and responsive to intracellular $\bullet\text{OH}$ concentration changes, with probe III producing the strongest fluorescence signal.

Detection of $\bullet\text{OH}$ in Cancer Cells. Expanding evidence suggests a link between free radicals and cancer.⁷ Accordingly, to examine the capacity of our probes to quantify $\bullet\text{OH}$ in cancer cells, we characterized these probes in SW620 (human colon cancer cells), Hela (human cervical cancer cells), and HepG2 cells (human hepatocellular liver carcinoma cells). Time-course analyses of probe uptake revealed rapid cellular access and stability over

(5) (a) Winkler, B. S.; Boulton, M. E.; Gottsch, J. D.; Sternberg, P. *Mol. Vis.* **1999**, *5*. (b) Beatty, S.; Koh, H. H.; Henson, D.; Boulton, M. *Surv. Ophthalmol.* **2000**, *45*, 115. (c) Cai, J. Y.; Nelson, K. C.; Wu, M.; Sternberg, P.; Jones, D. P. *Prog. Retin. Eye Res.* **2000**, *19*, 205.

(6) Takeuchi, T.; Nakajima, M.; Morimoto, K. *Carcinogenesis* **1996**, *17*, 1543.

(7) Hemnani, T.; Parihar, M. S. *Indian J. Physiol. Pharmacol.* **1998**, *42*, 440.

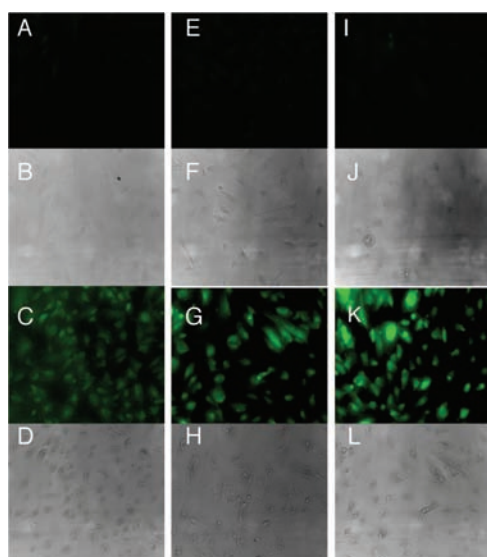


Figure 3. Fluorescence and DIC images of PMA (40 ng/mL) induced \bullet OH production in ARPE-19 cells using 2 μ M probe (I–III) for 12 h (pH 6) and 37 $^{\circ}$ C. Images for probe I alone (A and B); Images for probe I + PMA (C and D); Images for probe II alone (E and F); Images for probe II + PMA (G and H); Images for probe III alone (I and J); Images for probe III + PMA (K and L). All images were acquired with 20 \times objective lens.

time (Figures S7–S12). There were no indications of cell damage induced by probe loading. Along these lines, HepG2 cells display an epithelial-like morphology, and this morphology was maintained even after probe incubation for >24 h. Similar results were observed with spindle-shaped SW 620 cells; DIC imaging confirmed cellular viability, at up to a 32 μ M probe concentration. Counterstaining of cells (HepG2, SW-620 and Hela cells) with mitotracker and Hoechst 3342/DAPI (4',6-diamidino-2-phenylindole dihydrochloride) revealed that the predominant probe distribution was in the mitochondria, although some localization to the nucleus was also observed (Figure 4). These results suggest that the predominant site of \bullet OH generation is intramitochondrial, with only a slight production in the nuclear organelle.

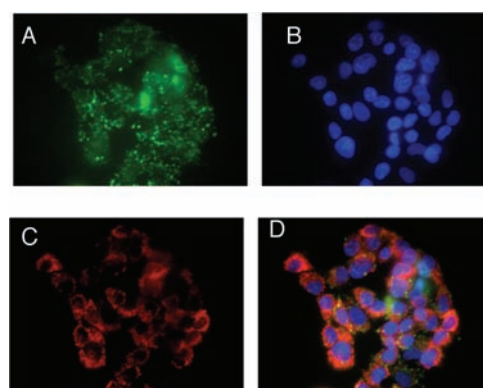


Figure 4. Fluorescence images of probe III in HepG2 cells. Probe III (30 μ M, green, A) was incubated in non-FBS media for 3 h and counterstained with Hoechst 3342 (1 μ g/mL, blue, B); mitotracker green (80 nM, red, C); and an overlay (D). All images were acquired with 40 \times objective.

In conclusion, we have developed new rhodamine nitroxide based fluorescent probes for intracellular \bullet OH imaging. The probes (I–III) exhibit excellent selectivity for \bullet OH, with good dynamic response ranges and micromolar detection limits for \bullet OH. Further, we have documented the utility of these probes for diverse applications in biological imaging, where our probes demonstrate high sensitivity and selectivity, good photostability, and cell membrane permeability. Our studies will facilitate further development of fluorescent probes that will aid in investigating the pathophysiology of \bullet OH toxicity in living cells and tissue.

Acknowledgment. L.B. is grateful to NASA (Grant MSGC R85197), Research Excellence Fund (Grant R01121) for support of this project. The authors at Columbia thank the National Science Foundation for support through Grant NSF-CHE-07-17518.

Supporting Information Available. Experimental details of synthesis, fluorescence spectroscopy, NMR data, and fluorescence imaging are provided as Supporting Information. This material is available free of charge via the Internet at <http://pubs.acs.org>.